arXiv:cond-mat/0409132v2 [cond-mat.stat-mech] 5 Jul 2005

Ground-state properties of hard-core bosons confined on one-dimensional optical lattices

Marcos Rigol and Alejandro Muramatsu
Institut für Theoretische Physik III, Universität Stuttgart, Pfaffenwaldring 57, D-70550 Stuttgart, Germany.

We study the ground-state properties of hard-core bosons trapped by arbitrary confining potentials on one-dimensional optical lattices. A recently developed exact approach based on the Jordan-Wigner transformation is used. We analyze the large distance behavior of the one-particle density matrix, the momentum distribution function, and the lowest natural orbitals. In addition, the low-density limit in the lattice is studied systematically, and the results obtained compared with the ones known for the hard-core boson gas without the lattice.

PACS numbers: 03.75.Hh, 05.30.Jp

I. INTRODUCTION

Low dimensional systems have been the subject of increasing interest over the past decades, traditionally in condensed-matter physics, and recently in the framework of quantum gases. There, recent advances in atom waveguide technology [1, 2, 3, 4, 5], the realization of quantum gases in very anisotropic traps [6, 7] and loading Bose-Einstein condensates (BEC) on optical lattices [8, 9, 10], allowed experimentalists to obtain a rich variety of systems where the reduced dimensionality rules the physics. Particularly interesting is the case in which the quantum dynamics of the system becomes quasi-one-dimensional. In that case it was shown [11, 12, 13] that in certain regimes of large scattering length, low densities, and low temperatures, bosons behave as impenetrable particles known as hard-core bosons (HCB's).

The one-dimensional (1D) homogeneous gas of HCB's was introduced by Girardeau [14], and a one-to-one correspondence between 1D HCB's and spinless fermions was established. It was shown later by Lenard and by Vaidya and Tracy [15, 16] that in homogeneous space, the 1D HCB gas does not exhibit true condensation at zero temperature since there is only off-diagonal quasi-long-range order (one-particle correlations decay as a power law), leading to an occupation of the lowest effective single-particle state (the highest occupied one) $\sim \sqrt{N_b}$, where N_b is the total number of HCB's.

Recently, theoretical studies have been focused on the ground-state properties of 1D HCB gases in the presence of harmonic potentials [17, 18, 19, 20, 21, 22], which are required in the experiments with quantum gases to keep the particles confined. Using the Fermi-Bose mapping, quantities like density profiles, momentum profiles, the natural orbitals (effective single-particle states), and the one-particle density matrix have been calculated for a finite number of particles. Some results were extended to the thermodynamic limit ($N_b \to \infty$) [21, 22]. It has been found that similarly to the homogeneous case the occupation of the lowest natural orbital is $\sim \sqrt{N_b}$ [20, 21], so that only a quasicondensate develops in the trap.

Another case of interest is given by HCB's on a lattice. These systems have been realized experimentally very recently [23]. In the periodic case, the 1D HCB Hamiltonian can be mapped into the 1D XY model of Lieb, Schulz, and Mattis [24]. This model has been extensively studied in the literature. At zero temperature the asymptotic behavior of the correlation functions is known [25, 26, 27]. In the presence of a confining potential, the systems realized experimentally in Ref. [23], the situation is more complicated. This is because the trapping potential is equivalent to the addition of a space-varying transverse field to the XY Hamiltonian, for which in general analytical results are not available.

In this work we study ground-state properties of 1D trapped HCB's in a lattice. The lattice opens new possibilities for engineering states that cannot be obtained in continuous systems. In particular, for HCB's it is possible to create pure Fock states when the occupation in some regions of the system reaches the value $n = 1$, such that coherence is lost there, and these sites decouple from the rest of the system. In addition, the properties of the systems without the lattice can be recovered in the low-density limit in a lattice. We follow a numerical approach, based on the Jordan-Wigner transformation [28], that allows us to calculate exactly the one-particle Green's function and analyze arbitrary confining potentials. This approach was recently introduced in Ref. [29] to study ground-state properties, and generalized in Ref. [30] for the study of the nonequilibrium dynamics.

We concentrate here on the behavior of the off-diagonal part of the one-particle density matrix, the momentum distribution function, and the natural orbitals. These quantities have a different behavior for HCB's when compared with spinless fermions to which the HCB Hamiltonian is mapped by means of the Jordan-Wigner transformation. We find that the one-particle density matrix (ρ_{ij}) decays as a power law $\sim |x_i - x_j|^{-1/2}$ for large distances, like in the periodic case [25], irrespective of the confining potential chosen. This is valid even when portions of the system reach occupation $n_i = 1$, such that coherence is lost there. The power law above is shown to determine the scaling of the occupation of the lowest natural orbital in the thermodynamic limit. This scaling and its finite-size corrections are also studied for ar-

bitrary powers of the confining potential. In addition, the low-density limit in the lattice is analyzed in detail and the results obtained are compared with the ones presented in Ref. [21] for continuous systems.

The exposition is organized as follows. In Sec. II we describe the numerical approach used. In Sec. III we discuss the properties of HCB's on periodic lattices. Systems confined in harmonic traps are analyzed in Sec. IV. In Sec. V we generalize to arbitrary powers of the confining potential the results obtained for the harmonic case. Finally, the conclusions are given in Sec. VI.

II. EXACT APPROACH

In the present section we describe in detail the exact approach we follow to study 1D HCB's in the presence of a lattice [29]. The HCB Hamiltonian can be written as

$$H = -t\sum_i \left(b_i^\dagger b_{i+1} + h.c.\right) + V_\alpha \sum_i x_i^\alpha\ n_i, \qquad (1)$$

with the addition of the on-site constraints

$$b_i^{\dagger 2} = b_i^2 = 0,\ \left\{b_i, b_i^\dagger\right\} = 1. \qquad (2)$$

These constraints on the creation ($b_i^\dagger$) and annihilation (b_i) operators avoid double or higher occupancy. Notice that the brackets in Eq. (2) apply only to on-site anticommutation relations, while $[b_i, b_j^\dagger] = 0$ for $i \neq j$, i.e., they commute on different sites [24]. In Eq. (1), the hopping parameter is denoted by t, and the last term describes an arbitrary confining potential, with power α and strength V_α; $n_i = b_i^\dagger b_i$ is the particle number operator.

In order to obtain the ground-state properties of HCB's, we use the Jordan-Wigner transformation [28],

$$b_i^\dagger = f_i^\dagger \prod_{\beta=1}^{i-1} e^{-i\pi f_\beta^\dagger f_\beta}, \quad b_i = \prod_{\beta=1}^{i-1} e^{i\pi f_\beta^\dagger f_\beta} f_i\ , \qquad (3)$$

which maps the HCB Hamiltonian into the noninteracting spinless fermions Hamiltonian

$$H = -t\sum_i \left(f_i^\dagger f_{i+1} + h.c.\right) + V_\alpha \sum_i x_i^\alpha\ n_i^f, \qquad (4)$$

where $f_i^\dagger$ and f_i are the creation and annihilation operators for spinless fermions and $n_i^f = f_i^\dagger f_i$ is their particle number operator. This means that HCB's and fermions have exactly the same spectrum. The nontrivial differences between both systems appear in the off-diagonal correlation functions as shown below.

Using the mapping above, the one-particle Green's function for the HCB's can be written in the form

$$\begin{aligned} G_{ij} &= \langle \Psi_{HCB}^G | b_i b_j^\dagger | \Psi_{HCB}^G \rangle \\ &= \langle \Psi_F^G | \prod_{\beta=1}^{i-1} e^{i\pi f_\beta^\dagger f_\beta} f_i f_j^\dagger \prod_{\gamma=1}^{j-1} e^{-i\pi f_\gamma^\dagger f_\gamma} | \Psi_F^G \rangle \\ &= \langle \Psi_F^A | \Psi_F^B \rangle, \end{aligned} \qquad (5)$$

where $|\Psi_{HCB}^G\rangle$ is the HCB ground-state wave function, and $|\Psi_F^G\rangle$ is the equivalent noninteracting fermion ground-state wave function. In addition, we denote

$$\begin{aligned} \langle \Psi_F^A | &= \left(f_i^\dagger \prod_{\beta=1}^{i-1} e^{-i\pi f_\beta^\dagger f_\beta} | \Psi_F^G \rangle \right)^\dagger, \\ |\Psi_F^B\rangle &= f_j^\dagger \prod_{\gamma=1}^{j-1} e^{-i\pi f_\gamma^\dagger f_\gamma} | \Psi_F^G \rangle. \end{aligned} \qquad (6)$$

The ground-state wave function of the equivalent Fermionic system can be obtained by diagonalizing Eq. (4) (the properties of such systems were analyzed in Ref. [31]), and can be written in the form

$$|\Psi_F^G\rangle = \prod_{\delta=1}^{N_f} \sum_{\sigma=1}^{N} P_{\sigma\delta} f_\sigma^\dagger\ |0\rangle, \qquad (7)$$

with N_f the number of fermions ($N_f = N_b$), N the number of lattice sites, and the matrix of the components $\mathbf{P}$ is given by the lowest N_f eigenfunctions of the Hamiltonian,

$$\mathbf{P} = \begin{pmatrix} P_{11} & P_{12} & \cdot & \cdot & \cdot & P_{1N_f} \\ P_{21} & P_{22} & \cdot & \cdot & \cdot & P_{2N_f} \\ \cdot & \cdot & \cdot & \cdot & \cdot & \cdot \\ \cdot & \cdot & \cdot & \cdot & \cdot & \cdot \\ \cdot & \cdot & \cdot & \cdot & \cdot & \cdot \\ P_{N1} & P_{N2} & \cdot & \cdot & \cdot & P_{NN_f} \end{pmatrix} \qquad (8)$$

In order to calculate $|\Psi_F^A\rangle$ (and $|\Psi_F^B\rangle$) we notice that

$$\prod_{\beta=1}^{i-1} e^{-i\pi f_\beta^\dagger f_\beta} = \prod_{\beta=1}^{i-1} \left[1 - 2\ f_\beta^\dagger f_\beta\right]. \qquad (9)$$

Then, the action of $\prod_{\beta=1}^{i-1} e^{-i\pi f_\beta^\dagger f_\beta}$ on the Fermionic ground state [Eq. (7)] generates only a change of sign on the elements $P_{\sigma\delta}$ for $\sigma \leq i-1$, and the further creation of a particle at site i implies the addition of one column to $\mathbf{P}$ with the element $P_{iN_f+1} = 1$ and all the others equal to zero (the same can be done for $|\Psi_F^B\rangle$). Then $|\Psi_F^A\rangle$ and $|\Psi_F^B\rangle$ can be written as

$$\begin{aligned} |\Psi_F^A\rangle &= \prod_{\delta=1}^{N_f'} \sum_{\sigma=1}^{N} P'^A_{\sigma\delta} f_\sigma^\dagger\ |0\rangle, \\ |\Psi_F^B\rangle &= \prod_{\delta=1}^{N_f'} \sum_{\sigma=1}^{N} P'^B_{\sigma\delta} f_\sigma^\dagger\ |0\rangle, \end{aligned} \qquad (10)$$

where $\mathbf{P'}^A$ and $\mathbf{P'}^B$ are obtained from $\mathbf{P}$ changing the required signs and adding the new column (N_f'=N_f+1).

The Green's function G_{ij} is then calculated as

$$\begin{aligned}\langle\Psi_F^A|\Psi_F^B\rangle &= \langle 0|\prod_{\delta=1}^{N_f'}\sum_{\sigma=1}^{N} P_{\sigma\delta}'^{A} f_\sigma \prod_{\bar{\delta}=1}^{N_f'}\sum_{\bar{\sigma}=1}^{N} P_{\bar{\sigma}\bar{\delta}}'^{B} f_{\bar{\sigma}}^\dagger\,|0\rangle \\ &= \sum_{\substack{\sigma_1,\cdots,\sigma_{N_f'}\\ \bar{\sigma}_1,\cdots,\bar{\sigma}_{N_f'}}}^{N} P_{\sigma_1 1}'^{A}\cdots P_{\sigma_{N_f'}N_f'}'^{A} P_{\bar{\sigma}_1 1}'^{B}\cdots P_{\bar{\sigma}_{N_f'}N_f'}'^{A} \\ &\quad\times\langle 0|f_{\sigma_1}\cdots f_{\sigma_{N_f'}} f_{\bar{\sigma}_{N_f'}}^\dagger\cdots f_{\bar{\sigma}_1}^\dagger|0\rangle \\ &= \det\left[\left(\mathbf{P}'^{A}\right)^\dagger \mathbf{P}'^{B}\right], \end{aligned} \tag{11}$$

where the following identity was used

$$\langle 0|f_{\sigma_1}\cdots f_{\sigma_{N_f'}} f_{\bar{\sigma}_{N_f'}}^\dagger\cdots f_{\bar{\sigma}_1}^\dagger|0\rangle = \epsilon^{\lambda_1\cdots\lambda_{N_f'}}\delta_{\sigma_1\bar{\sigma}_{\lambda_1}}\cdots\delta_{\sigma_{N_f'}\bar{\sigma}_{\lambda_{N_f'}}}, \tag{12}$$

with $\epsilon^{\lambda_1\cdots\lambda_{N_f'}}$ the Levi-Civita symbol in N_f' dimensions, the indices λ have values between one and N_f'.

The Green's function (11) is then evaluated numerically, and the one-particle density matrix is determined by the expression

$$\rho_{ij} = \left\langle b_i^\dagger b_j\right\rangle = G_{ij} + \delta_{ij}\left(1 - 2G_{ii}\right). \tag{13}$$

An alternative approach to the one presented here to calculate the one-particle density matrix of HCB's confined on optical lattices, using the Jordan-Wigner transformation, was followed by Paredes *et al.* [23]. In their work the elements of the one-particle density matrix were evaluated as Töplitz determinants of matrices with sizes up to $(N-1)\times(N-1)$. Within our approach only determinants of $(N_b+1)\times(N_b+1)$ matrices are evaluated.

III. HARD-CORE BOSONS ON PERIODIC SYSTEMS

In this section we analyze the properties of HCB's in 1D periodic lattices. In this case the Hamiltonian (1) can be written as

$$H = -t\sum_i\left(b_i^\dagger b_{i+1} + h.c.\right). \tag{14}$$

This Hamiltonian, with the additional constraints (2), is particle-hole symmetric under the transformation $h_i = b_i^\dagger$, $h_i^\dagger = b_i$. The operators $h_i^\dagger$ and h_i are the creation and annihilation operator for holes. The previous symmetry has important consequences since it implies that the off-diagonal elements of the one-particle density matrix for N_b HCB's $[\rho_{ij}(N_b)]$ and for $N-N_b$ HCB's $[\rho_{ij}(N-N_b)]$ are equal. Only the diagonal elements change, and they satisfy the relation $\rho_{ii}(N_b) = 1 - \rho_{ii}(N-N_b)$.

In the momentum distribution function (n_k), the particle-hole symmetry leads to

$$n_k(N_b) = n_{-k}(N-N_b) + \left(1 - \frac{N-N_b}{N/2}\right), \tag{15}$$

so that an explicit dependence on the density appears. This behavior is different from the one of noninteracting spinless fermions, where the Hamiltonian is also particle-hole symmetric but under the transformation $h_i' = (-1)^i f_i^\dagger$, $h_i'^\dagger = (-1)^i f_i$. In this case the momentum distribution function for fermions $[n_k^f(N_f)]$ and $[n_k^f(N-N_f)]$ are related by the expression

$$n_k^f(N_f) = 1 - n_{-k+\pi}^f(N-N_f), \tag{16}$$

where there is no explicit dependence on the density.

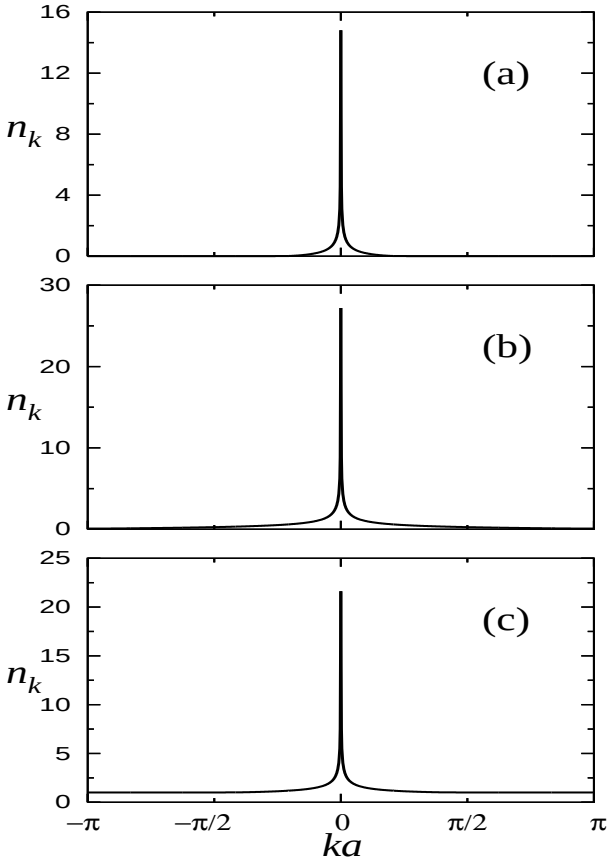


FIG. 1: Momentum profiles for periodic systems with 1000 lattice sites and occupations of 101 (a), 501 (b), and 799 (c) HCB's.

In Fig. 1 we show the momentum profiles for systems with three different fillings in 1000 lattice sites. Notice that we consider odd numbers of particles, which allows using periodic boundary conditions [24]. (In the case of an even number of particles antiperiodic boundary conditions are required [24].) The peak structure in the momentum distribution function (Fig. 1) reflects the Bosonic nature of the particles, and is in contrast with the structure of the momentum distribution function for the equivalent noninteracting fermions. On increasing the number of HCB's two effects can be seen: (i) up to half filling the value of $n_{k=0}$ increases, and it starts to decrease when the number of particles exceeds half filling; (ii) the population of high momenta states is always

increasing, showing that on increasing the density in the system, HCB's become more localized. The latter can be understood due to the impenetrability property of HCB's and the 1D character of the system.

A. Off-diagonal correlations and $n_{k=0}$

The formation of the peak in the momentum distribution function of the HCB's is due to the off-diagonal quasi-long-range correlations present in the one-particle density matrix. As is shown in Fig. 2 they decay as $\rho_x = A(\rho)/\sqrt{x/a}$ ($x = |x_i - x_j|$). $A(\rho)$ is a function of the density ($\rho = N_b/N$) in the system. A trivial calculation shows that in the thermodynamic limit, keeping the density constant, $n_{k=0} \sim 1/N \sum_{ij} |x_i - x_j|^{-1/2}$ scales as

$$n_{k=0} = B(\rho)\sqrt{N_b} = C(\rho)\sqrt{N}. \tag{17}$$

where $B(\rho)$ and $C(\rho)$ are functions of the density. The previous result is valid to a good approximation for finite systems (for occupations higher than 100 HCB's), as shown in the inset in Fig. 2 where we plot $n_{k=0}$ vs N_b for different systems at half filling. The straight line displays a $\sqrt{N_b}$ behavior.

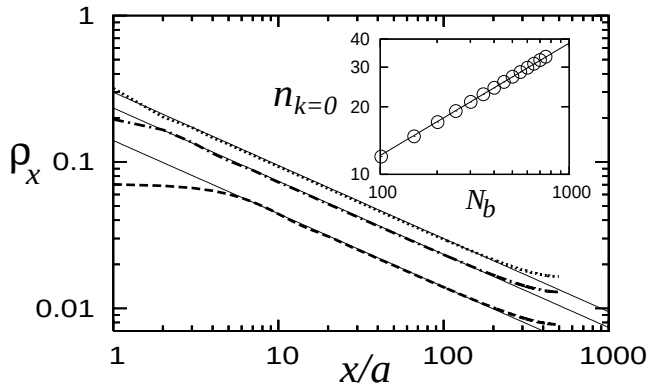


FIG. 2: One-particle density matrix ρ_x vs x/a for periodic systems with $N = 1000$ and $\rho = 0.5$ (dotted line), $\rho = 0.211$ (dashed-dotted line), $\rho = 0.071$ (dashed line). Thin continuous lines correspond to power laws $\sqrt{x/a}$. The inset shows $n_{k=0}$ vs N_b for systems at half filling (◯), the line exhibits $\sqrt{N_b}$ behavior.

A global picture of the occupation of the state with zero momentum as a function of the density is shown in Fig. 3. There we plot $n'_{k=0} = n_{k=0}/\sqrt{N}$ vs the density, and compare systems with 1000 and 300 lattice sites. The comparison shows that already for these system sizes the finite-size corrections are small. Actually, they are found to be given by

$$n_{k=0}/\sqrt{N} = C(\rho) - D(\rho)/\sqrt{N}, \tag{18}$$

where $D(\rho)$ can be positive or negative depending on the density. The inset in Fig. 3 shows $\delta n'_{k=0} = C(\rho) - n'_{k=0}$ vs $N^{-1/2}$ for half filled systems. The straight line displays the result of our fit for $C(\rho = 0.5)$ and $D(\rho = 0.5)$, and confirms the validity of Eq. (18). The same functional form of the finite-size corrections was obtained for the continuous case [21], which corresponds to systems in a lattice where the average interparticle distance is much larger than the lattice constant, i.e., in the limit $\rho = N_b/N \to 0$.

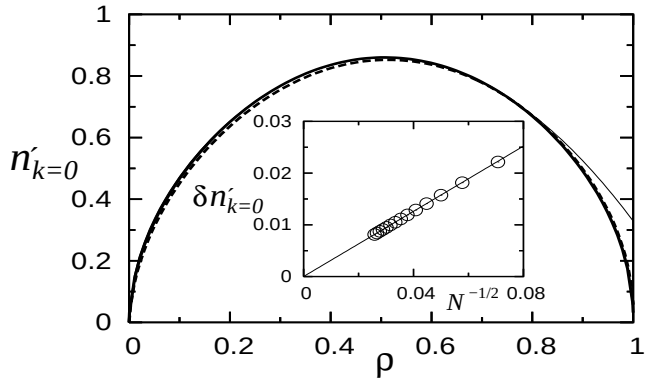


FIG. 3: Normalized occupation of $k = 0$ ($n'_{k=0}$) as a function of the density in periodic systems with $N = 1000$ (thick continuous line) and $N = 300$ (dashed line). The thin continuous line shows a fit of Eq. (21), with $b = 1.51$ and $c = 1.18$, to our numerical results for $N = 1000$. The inset displays $\delta n'_{k=0}$ vs $N^{-1/2}$ (see text) for half filled systems (◯), the straight line shows the result of our fit to Eq. (18).

B. Low-density limit in the lattice

In what follows we study the corrections introduced by the lattice to the occupation of the lowest momentum states in the continuous case. In a lattice at low momenta, the spectrum is quadratic in k and $\delta k \sim 1/N$, so that the ratio between the level spacing and the band width reduces proportionally to $1/N^2$ when N is increased. We find that the low-momentum occupations approach their values in the continuous case in exactly the same way,

$$\lambda_\eta(N_b, N) = \Lambda_\eta(N_b) - \frac{E_\eta(N_b)}{N^2}, \tag{19}$$

where $\lambda_\eta(N_b, N) \equiv n_{k=2\pi\eta/Na}(N_b)$ is the occupation of a momentum state η when there are N_b HCB's in a system with N lattice sites. $\Lambda_\eta(N_b)$ is the occupation of the momentum state η in the continuous case, and $E_\eta(N_b)$ for a given η is a function of N_b.

We obtain $\Lambda_\eta(N_b)$ and $E_\eta(N_b)$ for the three lowest momenta states analyzing systems with fillings up to 501 particles and sizes up to 2000 lattice sites. In Fig. 4, we compare our results for $\Lambda_\eta(N_b)$ with the ones in the continuous case presented in Ref. [21] [see Eqs. (56)–(58) there]. The agreement is excellent. In the inset we plot $\Delta\lambda = \Lambda_\eta(N_b) - \lambda_\eta(N_b, N)$ also for the three lowest momentum states as a function of $1/N^2$ confirming Eq. (19).

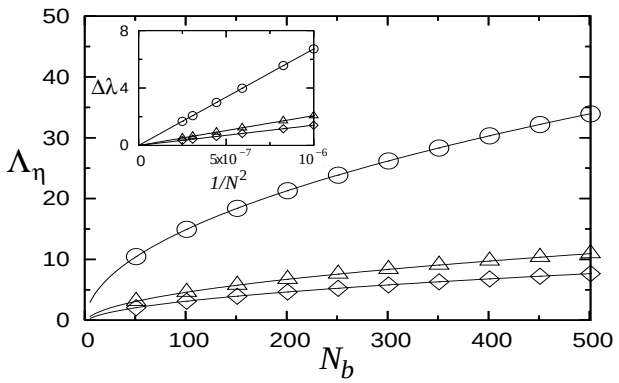


FIG. 4: Extrapolated values of the first (◯), second (△), and third (◇) momentum-state occupations in the continuous case (Λ_η). The lines following the data correspond to the results obtained in Ref. [21]. The inset shows $\Delta\lambda$ (see text) vs $1/N^2$ also for the first (◯), second (△), and third (◇) momenta states in systems with 501 HCB's and sizes between 1000 and 2000 lattice sites, the straight lines are the result of our fits.

Surprisingly, we find that Eq. (19) works extremely well up to very high densities ($n \sim 0.8$). This feature allows one to understand the dependence of the lowest natural orbital occupation on the density (Fig. 3) as follows.

The dependence of $\Lambda_0\,(N_b)$ and $E_0\,(N_b)$ on N_b can be determined given Eq. (17) to be

$$\Lambda_0\,(N_b) = b\,\sqrt{N_b}, \qquad E_0\,(N_b) = c\,N_b^{5/2}, \tag{20}$$

where b and c are two constants that can be obtained numerically. (Both relations above were confirmed by our numerical results.) Then Eq. (19) may be rewritten as

$$\lambda_0\,(N,\rho)\,/\sqrt{N} = \sqrt{\rho}\,(b - c\,\rho^2)\,. \tag{21}$$

A fit of Eq. (21) to our numerical results for $N = 1000$, with $b = 1.51$ and $c = 1.18$, is shown in Fig. 3 as a thin continuous line. As it can be seen, Eq. (21) describes very well the numerical results up to densities $n \sim 0.8$, which were the densities up to which we had found that Eq. (19) was a good approximation.

C. $n_{k=0}$ singularity in the thermodynamic limit

To conclude this section on periodic systems, we analyze in detail the low-momentum region of the momentum distribution function. The power-law decay of the one-particle density matrix ($\rho_x \sim 1/\sqrt{x/a}$) implies that in the thermodynamic limit the momentum distribution function has a $|k|^{-\beta}$ ($\beta = 1/2$) singularity at $k = 0$ [16]. For finite systems we find that, due to finite-size effects, the apparent exponent observed in the low-momentum region of n_k depends strongly on the number of particles in the system. In Fig. 5 we show a log-log plot of the momentum distribution of two systems at half filling with $N = 100$ and $N = 1000$ lattice sites. A fit to a power law in the case of 100 lattice sites reveals an exponent $\beta = 0.63$. As the figure shows, the increase of the system size reduces the exponent of the power law only in the low-momentum region. We have studied systems at half filling fitting power laws from the lowest ten momentum states available (excluding $k = 0$). The results are shown in the inset of Fig. 5. This inset shows that with increasing the system size the exponent β extrapolates very slowly to 0.5. Basically, we find that it extrapolates as a power law $\sim N^{-0.63}$. The latter exponent is a nonuniversal one since it depends on the way in which one fits power laws for the low-momentum region of n_k. Up to the bigger system we calculated $N = 1500$, the exponent β reduced only up to 0.523. Our results imply that the experimental observation of the thermodynamic limit exponent $\beta = 0.5$ will be very difficult if not impossible considering finite-temperature effects [23].

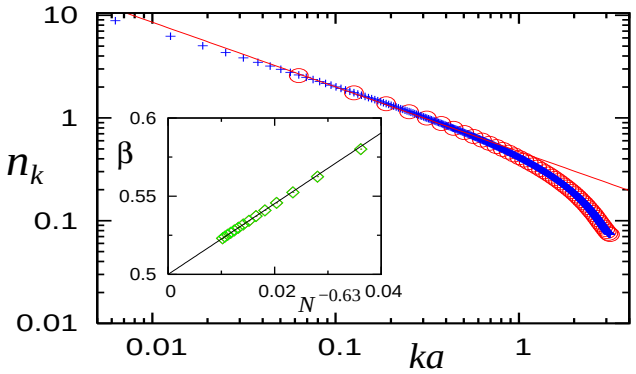


FIG. 5: (Color online) Log-log plot of the momentum distribution function of systems at half filling with $N = 100$ (◯) and $N = 1000$ (+) lattice sites. The straight line shows a power-law fit $n_k \sim k^{-\beta}$ ($\beta = 0.63$) to the lowest momentum states of the system with $N = 100$. The inset displays the dependence of the exponent β (fitted for half filled systems) on the system size. The straight line shows that it extrapolates to $\beta = 0.5$ for $N \to \infty$.

IV. HARD-CORE BOSONS CONFINED IN HARMONIC TRAPS

We analyze in this section the case in which HCB's are confined in harmonic traps. The Hamiltonian in this case is given by Eqs. (1) and (2) with $\alpha = 2$, and is not particle-hole symmetric like in the periodic case. In order to quantitatively characterize these systems we make use of the length scale set by the combination lattice-confining potential $\zeta = (V_\alpha/t)^{-1/2}$, and the associated characteristic density $\tilde{\rho} = N_b/\zeta$, both introduced in Refs. [31, 32, 33]. Since the diagonal elements of the one-particle density matrix for HCB's and the equivalent fermions are equal [see Eq. (5) for $i = j$], density properties of both systems trivially coincide. We concentrate here in the quantities related to the off-diagonal correlations of the HCB's, like the momentum distribution function and the natural orbitals.

The natural orbitals (ϕ_i^η) are defined as the eigenfunctions of the one-particle density matrix [34],

$$\sum_{j=1}^{N} \rho_{ij}\phi_j^\eta = \lambda_\eta \phi_i^\eta, \tag{22}$$

and can be understood as being effective single-particle states with occupations λ_η. The lowest natural orbital (the highest occupied one) is considered to be the condensate. In the periodic case the natural orbitals are plane waves, i.e, the eigenfunctions of Eq. (22) are momentum states (the lowest natural orbital is the state with momentum zero). On the contrary, since in the trapped case the translational invariance is broken, the natural orbitals occupations and the momentum distribution function do not coincide.

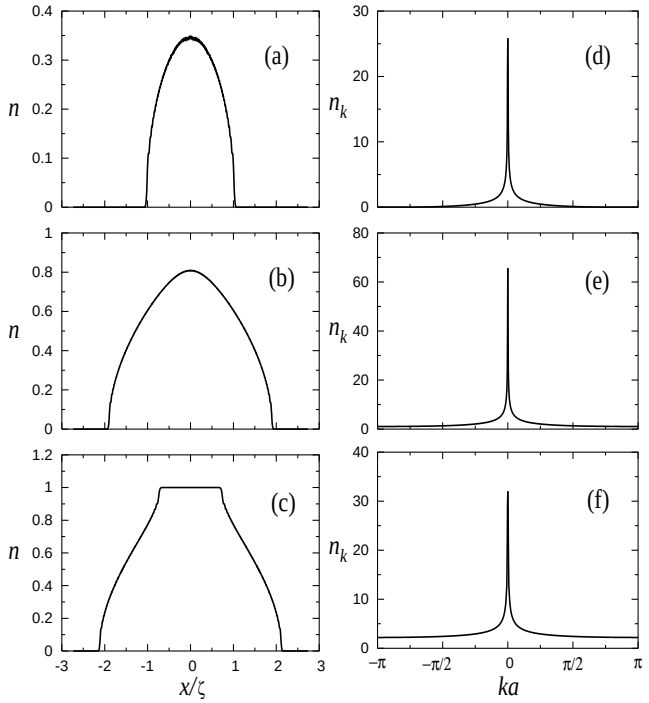


FIG. 6: Density (a)–(c) and normalized momentum distribution function (d)–(f) for trapped systems with 1000 lattice sites, $V_2a^2 = 3 \times 10^{-5}t$ and occupations of 101 (a),(d), 401 (b),(e), and 551 (c),(f) HCB's.

In Fig. 6 we show three density profiles and their corresponding normalized momentum distribution function for traps with 1000 lattice sites. Positions are normalized by the characteristic length ζ, and the normalized momentum distribution function is defined as $n_k = (a/\zeta)\sum_{ij=1}^{N} e^{-ik(i-j)}\langle b_i^\dagger b_j\rangle$. Figure 6 displays features similar to the periodic case. The normalized momentum distribution function exhibits narrow peaks at $k = 0$ with $n_{k=0}$ initially increasing with the number of particles, and decreasing after certain filling when more particles are added to the system. Localization effects also start to be evident at high fillings, with an increment of the population of high momenta states [Fig. 6(f)], and the formation of Fock states (or a Mott insulating plateau) in the middle of the system [sites with $n_i = 1$ in Fig. 6(c)]. Notice that in the latter case the formation of the Mott insulator did not destroy the sharp peak observed at $n_{k=0}$, which is associated to the superfluid phase surrounding the Mott plateau.

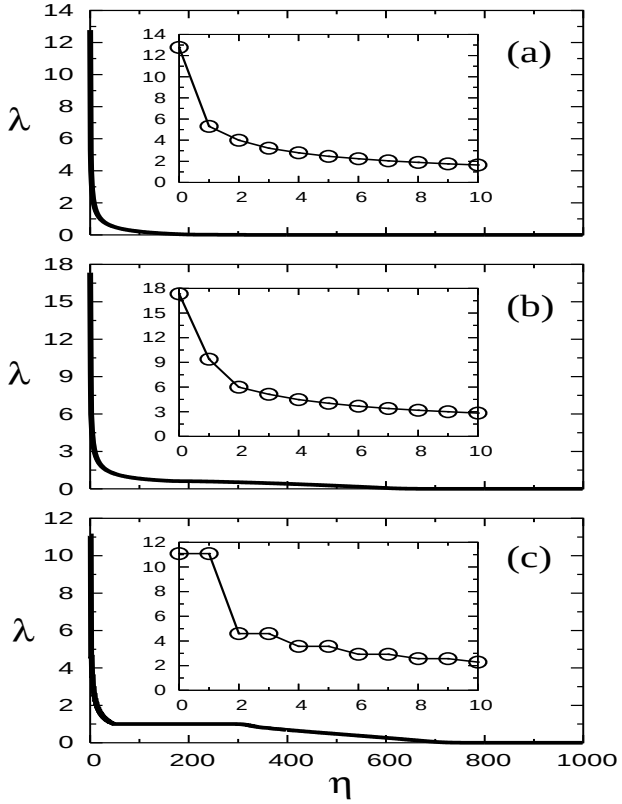


FIG. 7: Occupation of the natural orbitals for trapped systems with 1000 lattice sites, $V_2a^2 = 3 \times 10^{-5}t$, and occupations of 101 (a), 401 (b), and 551 (c) HCB's. The insets show the occupation of the lowest eleven natural orbitals in each case.

Results obtained for the occupations of the natural orbitals, in the systems of Fig. 6, are presented in Fig. 7. The occupations are plotted as a function of the orbital numbers η, and they are ordered starting from the highest one. The effects of increasing the filling in the system are similar to the ones observed in the momentum distribution function. The occupation of the lowest natural orbital increases with increasing the number of particles up to a certain filling where it starts to decrease when more particles are added. In contrast to the momentum distribution function, the natural orbital occupations exhibit clear signatures of the formation of the Mott insulating state in the middle of the system since a plateau with $\lambda = 1$ appears [Fig. 7(c)], and the natural orbitals with $\lambda \neq 1$ become pairwise degenerated [inset in Fig. 7(c)]. This can be easily understood since in the region where $n_i = 1$, the one-particle density matrix is diagonal $\rho_{ij} = \delta_{ij}$, so that it can be seen as a three block diagonal matrix with the block in the middle being an identity

matrix and the other two being identical. Thus the diagonalization gives a group of eigenvalues $\lambda_\eta = 1$ and all the others pairwise degenerated.

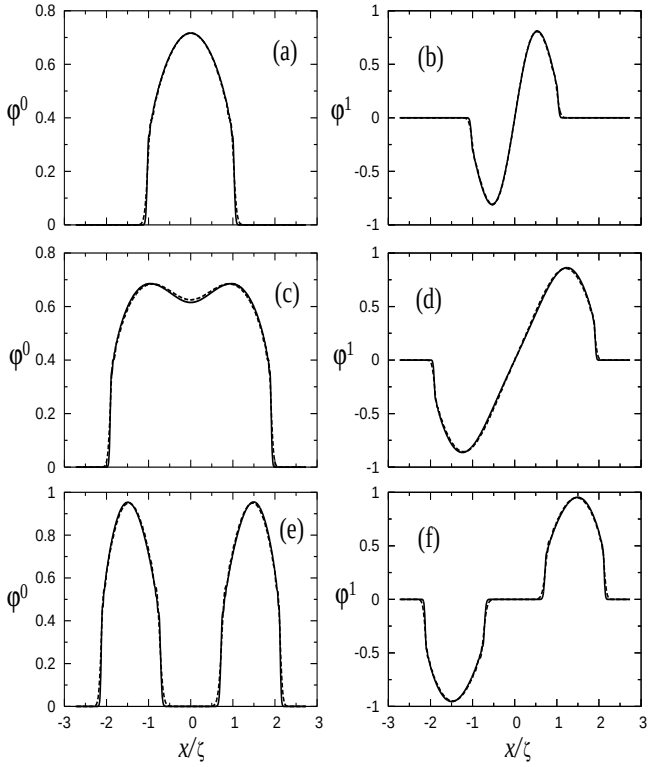


FIG. 8: Profiles of the two lowest natural orbitals for trapped systems with: 1000 lattice sites, $V_2a^2 = 3 \times 10^{-5}t$, and occupations of 101 (a),(b), 401 (c),(d), and 551 (e),(f) HCB's (continuous line); 300 lattice sites, $V_2a^2 = 3.3 \times 10^{-4}t$, and occupations of 30 (a),(b), 121 (c),(d), and 167 (e),(f) HCB's (dashed line).

Profiles of the two lowest natural orbitals, for the same parameters of Figs. 6 and 7, are presented in Fig. 8. Positions in the trap are also normalized by ζ and the proper definition of the scaled natural orbitals is given by

$$\varphi^\eta = R^{1/2}\phi^\eta, \qquad R = (N_b\zeta/a)^{1/2}. \tag{23}$$

This scaling relation is valid only for the lowest natural orbitals and is meaningful for comparing systems with the same characteristic density. Notice that for a given $\tilde{\rho}$ the occupied system size (L) is proportional to ζ, i.e, $L = F(\tilde{\rho})\zeta$ with $F(\tilde{\rho})$ depending only on the value of $\tilde{\rho}$. In Fig. 8 we have also plotted results for smaller systems (dashed line) but fulfilling the condition of equal characteristic density. The comparison between the plots shows that the scaling relation defined by Eq. (23) holds. (We find this to be valid to a good approximation for occupied system sizes larger than 100 lattice sites.) In Figs. 8(a) and (b) it can be seen that for low characteristic densities the natural orbitals are similar to the ones of systems without the optical lattice [20, 21]. On increasing the characteristic density the shape of the lowest natural orbital starts to change since its weight starts to reduce in the middle of the trap, as shown in Fig. 8(c). Once the Mott insulating plateau appears in the center of the system, degeneracy sets in for the lowest natural orbital [inset in Fig. 7(c)], and their weight in the region with $n = 1$ vanishes [Figs. 8(e) and (f)].

A. Off-diagonal correlations and the lowest natural orbital occupation

The peaks appearing in the momentum distribution function at $k = 0$, and the high occupation of the lowest natural orbitals are consequences of the off-diagonal quasi-long-range correlations present in the one-particle density matrix (ρ_{ij}). We obtain that away from $n_i, n_j = 0, 1$, ρ_{ij} decays as a power law $\rho_{ij} \sim |(x_i - x_j)/a|^{-1/2}$ for large distances independently of the fact that the density is changing in the system. This is shown in Fig. 9 where we plot ρ_{ij} for traps with fillings ranging over three decades. As an approximation, one may consider that ρ_{ij} and $|(x_i - x_j)/a|^{-1/2}$ are related through a constant that depends only on the characteristic density $\tilde{\rho}$, which in trapped systems plays a role similar to that played by the density in periodic systems.

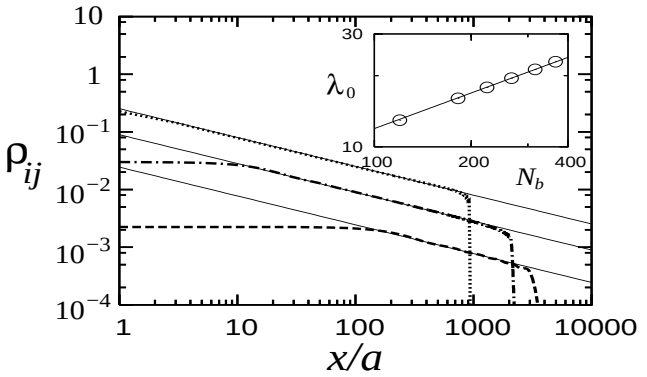


FIG. 9: HCB one-particle density matrix vs x/a ($x =\mid x_i - x_j \mid$) for systems with $N_b = 1000$, $\tilde{\rho} = 2.0$, $n_i = 0.75$ (dotted line), $N_b = 100$, $\tilde{\rho} = 4.47 \times 10^{-3}$, $n_i = 0.03$ (dashed-dotted line), and $N_b = 11$, $\tilde{\rho} = 2.46 \times 10^{-5}$, $n_i = 2.3 \times 10^{-3}$ (dashed line). The point i was chosen in the middle of the trap and only j was changed. The abrupt reduction of ρ_{ij} occurs for $n_j \to 0$. Thin continuous lines correspond to power laws $\sqrt{x/a}$. The inset shows λ_0 vs N_b for systems with $\tilde{\rho} = 1.0$ (◯). The straight line exhibits $\sqrt{N_b}$ behavior.

A detailed study shows, however, that ρ_{ij} and $|(x_i - x_j)/a|^{-1/2}$ are related by a slowly varying (away from $n_i, n_j = 0, 1$) function of the density, which we denote as $f_2(n_i, n_j)$. We find this function to be

$$f_2(n_i, n_j) \sim [n_i(1 - n_i)n_j(1 - n_j)]^{1/4}. \tag{24}$$

In order to show it, we plot in Fig. 10

$$\rho'_{ij} = \rho_{ij}|(x_i - x_j)/a|^{1/2}/[n_i(1 - n_i)]^{1/4} \tag{25}$$

vs n_j for two different values of n_i in a system where a Mott insulator is formed in the middle of the trap. (In

this case the density in the superfluid phase changes between 0 and 1.) The results for ρ'_{ij} are then compared with a function $A[n_j(1-n_j)]^{1/4}$, where as a fit we obtain $A = 0.58$. The agreement between the plots shows that $f_2(n_i, n_j)$ in Eq. (24) describes very well the density dependence of the one-particle density matrix in harmonically trapped systems.

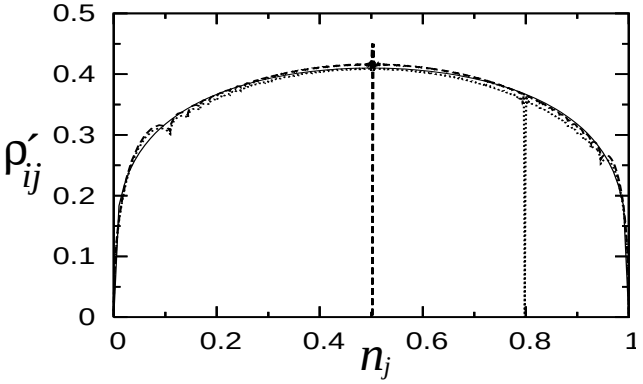


FIG. 10: HCB one-particle density matrix ρ'_{ij} [as in Eq. (25)] vs n_j. ρ'_{ij} is measured from points i with $n_i = 0.5$ (dashed line) and $n_i = 0.8$ (dotted line) in a trap with $N_b = 951$, $\tilde{\rho} = 2.61$ so that a Mott insulator is formed in the middle of the system. The thin continuous line corresponds to $0.58[n_j(1-n_j)]^{1/4}$.

The fact that the dependence of ρ_{ij} on the density is very small (a fourth root of the densities) is what allows one to observe the $|(x_i - x_j)/a|^{-1/2}$ behavior without the need of normalizing the one-particle density matrix. For very low characteristic densities ($n_i, n_j \to 0$) the function $f_2(n_i, n_j)$ reduces to the exact result known for the continuous case $f_2(n_i, n_j) \sim (n_i n_j)^{1/4}$ [21, 22]. In Fig. 11 we compare results obtained for ρ_{ij} and its normalized version,

$$\rho^N_{ij} = \rho_{ij}/[n_i(1-n_i)n_j(1-n_j)]^{1/4}. \qquad (26)$$

The difference between the power-law decay in both cases is small and can be only distinguished at very large distances. In addition, we have also plotted the results obtained for ρ_{ij} normalized following Kollath *et al.* [35],

$$\rho^K_{ij} = \rho_{ij}/\sqrt{n_i n_j}. \qquad (27)$$

As Fig. 11 shows for the HCB case, a possible power-law behavior in ρ^K_{ij} disappears much before the one observed in ρ_{ij} without normalization. This implies that the scaling of the correlations chosen in Ref. [35] does not apply to very strong Hubbard repulsions.

Considering the results for the power-law decay of the one-particle density matrix and for the scaling of the lowest natural orbital, it is possible to calculate how the lowest natural orbitals occupation scales in the thermodynamic limit ($\lambda_0 = \sum_{ij} \phi^0_i \rho_{ij} \phi^0_j$) defined by a constant

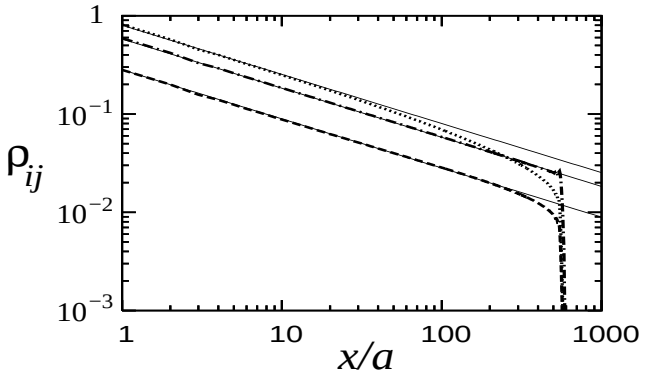


FIG. 11: One-particle density matrix normalized in different ways (for the same system) vs x/a ($x = |\, x_i - x_j \,|$): ρ_{ij} (dashed line), ρ^N_{ij} as in Eq. (26) (dashed-dotted line), and ρ^K_{ij} as in Eq. (27) (dotted line). Thin continuous lines exhibit $|x_i - x_j|^{-1/2}$ behavior. The plots were made for trap with $N_b = 951$ and $\tilde{\rho} = 2.61$ so that a Mott insulator is formed in the middle of the system. In addition, i was fixed ($n_i = 0.34$), and j was changed with $n_j > n_i$.

characteristic density. Replacing the sums in λ_0 by integrals ($L \gg a$),

$$\lambda_0 \sim 1/a^2 \int_{-L}^{L} dx \int_{-L}^{L} dy \frac{\phi^0(x) f_2[n(x), n(y)] \phi^0(y)}{|(x-y)/a|^{1/2}}$$
$$= (\zeta/a)^{3/2} R^{-1} \int_{-F(\tilde{\rho})}^{F(\tilde{\rho})} \int dX dY \frac{\varphi^0(X) f_2[n(X), n(Y)] \varphi^0(Y)}{|X-Y|^{1/2}}$$
$$= B_2(\tilde{\rho}) \sqrt{N_b} = C_2(\tilde{\rho}) \sqrt{\zeta/a}\ , \qquad (28)$$

where we did the change of variables $x = X\zeta$, $y = Y\zeta$, and $\phi^0 = R^{-1/2}\varphi^0$. The integral over X, Y depends only on the characteristic density. This is so because we have shown before that the scaled natural orbitals as a function of x/ζ do not change when the characteristic density is kept constant. In addition, also the density profiles (as a function of x/ζ) do not change when the characteristic density is kept constant. This feature, which is valid for HCB's and spinless fermions, was proven in Ref. [33]. Hence $B_2(\tilde{\rho})$ and $C_2(\tilde{\rho})$ depend only on $\tilde{\rho}$. The previous results show that with the properly defined characteristic density, the occupation of the lowest natural orbital scales like in the homogeneous case, proportionally to $\sqrt{N_b}$. Equation (28) is valid to a good approximation for finite systems, as can be seen in the inset in Fig. 9 where we plot λ_0 vs N_b for different systems with characteristic density $\tilde{\rho} = 1$, the straight line displays a $\sqrt{N_b}$ behavior.

A global picture of the occupation of the two lowest natural orbitals is shown in Fig. 12. There we plot $\lambda' = \lambda/\sqrt{\zeta/a}$ vs $\tilde{\rho}$, and compare systems with different curvatures of the confining potential. The Mott insulator forms in the middle of the trap when the degeneracy appears in the natural orbitals. The comparison between the plots shows that already for these system sizes (larger than 100 lattice sites) the finite-size corrections are small.

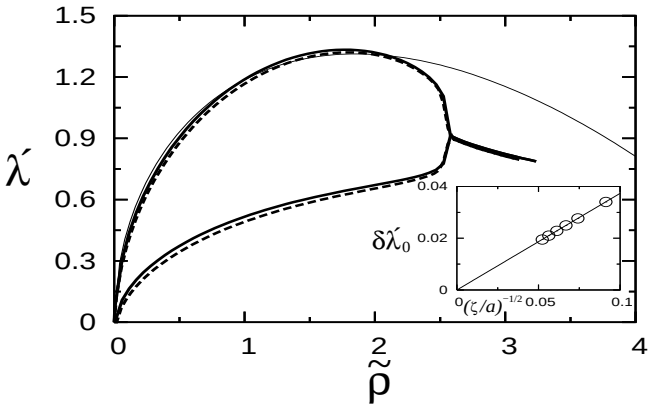


FIG. 12: Normalized occupation of the two lowest natural orbitals (see text) vs $\tilde{\rho}$. The systems analyzed have $N = 1000$, $V_2a^2 = 3 \times 10^{-5}t$, and occupations up to 600 particles (thick continuous line), and $N = 300$, $V_2a^2 = 3.3 \times 10^{-4}t$, and occupations up to 270 particles (dashed line). The thin continuous line shows a fit of Eq. (32), with $b_2 = 1.44$ and $c_2 = 0.26$, to our numerical results for $N = 1000$. The inset displays $\delta\lambda_0'$ vs $N^{-1/2}$ (see text) for traps with $\tilde{\rho} = 1$ (◯), the straight line shows the result of our fit to Eq. (29).

They were found to be determined by the expression

$$\lambda_0/\sqrt{\zeta/a} = C_2(\tilde{\rho}) - D_2(\tilde{\rho})/\sqrt{\zeta/a}, \qquad (29)$$

with $D_2(\tilde{\rho})$ being a function of the characteristic density. Equation (29) has the same form as Eq. (18) for the homogeneous case, when N is substituted by ζ/a. In the inset in Fig. 12, we plot $\delta\lambda_0' = C_2(\tilde{\rho}) - \lambda_0'$ vs $N^{-1/2}$ for systems with $\tilde{\rho} = 1$. The straight line displays the result of our fit for $C_2(\tilde{\rho} = 1)$ and $D_2(\tilde{\rho} = 1)$, and confirms the validity of Eq. (29). In the case without the lattice [21], the same functional form was obtained for the finite-size corrections in terms of the number of HCB's in harmonic traps.

B. Formation of the Mott insulator

So far we have analyzed generic features of harmonically trapped systems in a lattice. In what follows we study in more detail the formation of the Mott-insulating state in the middle of the trap. In Fig. 9 we have shown the behavior of the one-particle density matrix in systems with fillings below the one at which the Mott insulator appears in the middle of the trap, and once the Mott insulator has formed, splitting the trap in two parts. In all these cases power-law decays $\rho_{ij} \sim |x_i - x_j|^{-1/2}$ are observed. We find that when the local density approaches to one in the middle of the trap, the power law $\rho_{ij} \sim |x_i - x_j|^{-1/2}$ observed in one half of the system starts to disappear on entering in the other half. This effect can be seen in Fig. 13 where we plot ρ_{ij}^N [Eq. (26)] vs $|x_i - x_j|$ (for fixed i in one side of the trap) when the density in the middle of the system $n \to 1$. The density profiles corresponding to these density matrices are presented in the inset. The fast decay of the one-particle density matrix when crossing the middle of the trap (for $n \to 1$ in the center of the system) leads to the formation of two independent and identical quasicondensates in each side of the trap. This is reflected in Fig. 12 since the occupation of the two lowest natural orbitals starts to be similar on approaching the formation of the Mott insulating state.

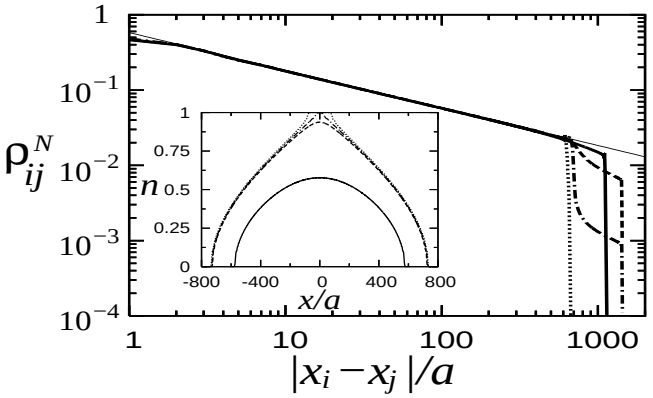


FIG. 13: HCB one-particle density matrix ρ_{ij}^N [Eq. (26)] on approaching the Mott insulating state. In the plots the trap curvature was kept constant $V_2a^2 = 7.5 \times 10^{-06}t$, and the filling was increased: $N_b = 500$ (thick continuous line), $N_b = 911$ (dashed line), $N_b = 931$ (dashed-doted line), and $N_b = 951$ (dotted line). The corresponding density profiles are shown in the inset. The thin continuous line following ρ_{ij}^N corresponds to a power law $0.58(|x_i - x_j|/a)^{-1/2}$. ρ_{ij}^N was measured in the four cases displayed fixing i so that $n_i \sim 0.2$.

In Fig. 13 we have also plotted a case where the density in the middle of the system is $n \sim 0.58$ (thick continuous line). In this case one can observe very small deviations from the $|x_i - x_j|^{-1/2}$ behavior in one half of the system on entering in the other half. This shows that although the destruction of quasi-long-range correlations between the two halves of the trap occurs only when the density in the middle of the system approaches $n_i = 1$, deviations from the power law $|x_i - x_j|^{-1/2}$ are observed before. They just increase with increasing the density in the middle of the trap. Only in the case of very low characteristic densities is the power law $|x_i - x_j|^{-1/2}$ observed in the whole system as shown in Fig. 14. A comparison between Figs. 13 and 14 reveals an interesting feature, which is also present in the homogeneous case (Fig. 2). The interface between the short-distance and large-distance behavior of the one-particle density matrix moves toward shorter distances with increasing the density in the system.

The destruction of the power-law decay of ρ_{ij} observed in Fig. 13 is reflected by an increase of the full width at half maximum of the momentum distribution function (w) close before the Mott insulator appears in the middle of the system. w is proportional to the inverse of the correlation length in the system. In the HCB case the

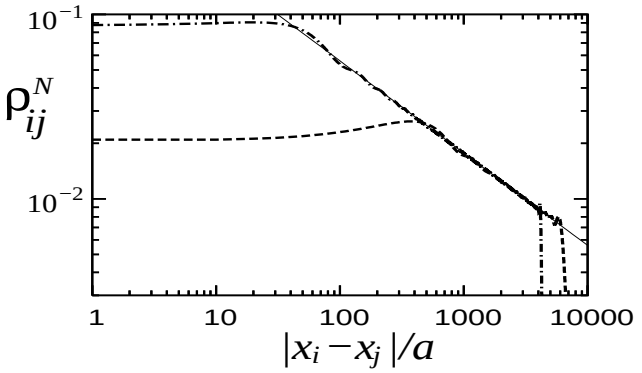


FIG. 14: HCB one-particle density matrix ρ_{ij}^N [Eq. (26)] for very dilute systems with $N_b = 100$, $\tilde{\rho} = 4.47 \times 10^{-3}$ (dashed-dotted line), and $N_b = 11$, $\tilde{\rho} = 2.46 \times 10^{-5}$ (dashed line). The thin continuous line following ρ_{ij}^N corresponds to a power law $0.56(|x_i - x_j|/a)^{-1/2}$. ρ_{ij}^N was measured in both cases displayed fixing i in one border of the trap.

correlation length is zero in the Mott-insulating phase and proportional to the size of the region $0 < n < 1$ for the superfluid phase. This implies that on filling the trap w starts to reduce (the system size increases) up to the point at which the system begins to split close before the formation of the Mott insulating state in the middle of the trap. This can be seen in Fig. 15 where we plot w as a function of the characteristic density for different system sizes. The points at which the Mott insulator appears are signaled by an arrow ($\tilde{\rho} \sim 2.6 - -2.7$). The figure also shows that, as it can be intuitively expected, the increase of w becomes smaller on increasing the system size since the superfluid phase (the one producing the peak) becomes larger. The proposal of measuring w

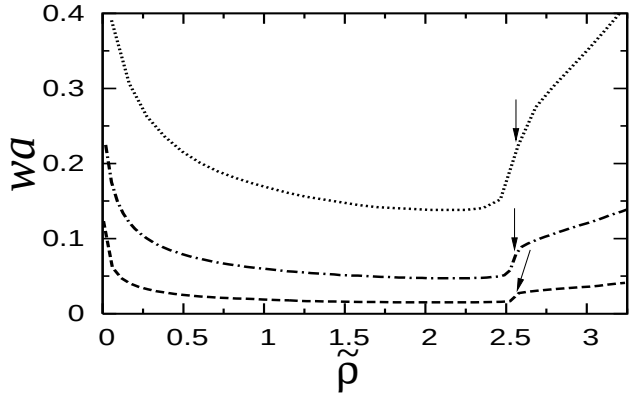


FIG. 15: Full width at half maximum of the momentum distribution function (w) as a function of the characteristic density for three different traps with $V_2 a^2 = 3.0 \times 10^{-3} t$ (dotted line), $V_2 a^2 = 3.3 \times 10^{-4} t$ (dashed-dotted line), and $V_2 a^2 = 3.0 \times 10^{-5} t$ (dashed line). The arrows signal the point at which the Mott insulator sets in the middle of the trap. In the plot w was normalized by the lattice constant a.

in order to (approximately) detect the parameter region where the local Mott insulator appears in the trap was done by Kollath *et al.* [35] for 1D systems and discussed by Wessel *et al.* [36] for higher dimensional systems. As it was shown by recent experimental results [10] for the systems sizes available experimentally w gives a signal of when the Mott insulator appears for the soft-core boson case. Since local Mott-insulating and superfluid phases coexist, in order to unambiguously characterize these systems local probes are needed. This has been discussed in Refs. [36, 37] for soft-core bosons and Refs. [32, 33] for fermions. The basic idea of local probes follows from the fact that the superfluid phases are compressible while the Mott insulating phases are incompressible (a gap opens in the charge excitations). However, such local probes have not been yet implemented experimentally.

C. Low-density limit in the lattice

Finally, we study the corrections introduced by the lattice to the occupation of the lowest natural orbitals in the confined continuous case. Due to the combination lattice-harmonic potential the ratio between the level spacing and the bandwidth in the low-energy region is proportional to $(\zeta/a)^{-1}$. As in the periodic case, we find that the occupation of the lowest natural orbitals approach their value in the continuous system $\Lambda_\eta(N_b)$ in the same way,

$$\lambda_\eta(N_b, \zeta/a) = \Lambda_\eta(N_b) - \frac{E_\eta^2(N_b)}{\zeta/a}, \tag{30}$$

where $\lambda_\eta(N_b, \zeta/a)$ is the occupation in a lattice for a given N_b and ζ, and $E_\eta^2(N_b)$ is a function of the number of particles for each η.

We calculate $\Lambda_\eta(N_b)$ and $E_\eta^2(N_b)$ for the three lowest natural orbitals analyzing systems with fillings up to 401 particles and sizes up to 2000 lattice sites. In Fig. 16 we

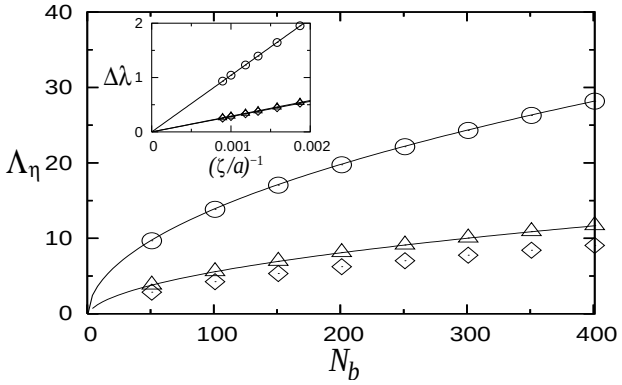


FIG. 16: Extrapolated values of the first (◯), second (△), and third (◇) natural orbital occupations in the continuous system (Λ_0). The lines following the data for the first two natural orbitals correspond to the results obtained in Ref. [21]. The inset shows $\Delta\lambda$ (see text) as a function of $(\zeta/a)^{-1}$ also for the first (◯), second (△), and third (◇) natural orbitals in systems with 301 HCB's and sizes between 1000 and 2000 lattice sites, the straight lines are the result of our fits.

compare our results for $\Lambda_\eta\,(N_b)$ with the ones presented in Ref. [21] for the continuous case [see Eqs. (91) and (92) there]. The agreement is excellent like in the periodic case. As an inset we plot $\Delta\lambda = \Lambda_\eta\,(N_b) - \lambda_\eta\,(N_b, \zeta/a)$ also for the three lowest natural orbitals as a function of $(\zeta/a)^{-1}$ confirming Eq. (30). (The results obtained for $\Delta\lambda$ for the second and third natural orbitals are very similar, so in the inset they are one on top of the other.) We find that Eq. (30) describes our numerical results up to characteristic densities very close to the the one at which the Mott insulator appears in the middle of the trap. Hence the dependence of the lowest natural orbital occupation on the density in Fig. 12 can be understood as follows.

Comparing Eqs. (30) and (28), it is possible to determine the dependence of $\Lambda_0\,(N_b)$, [21] and $E_0^2\,(N_b)$ on N_b

$$\Lambda_\eta\,(N_b) = b_2\ \sqrt{N_b}, \qquad E_\eta^2\,(N_b) = c_2\ N_b^{3/2}, \qquad (31)$$

where b_2, c_2 are parameters that can be determined numerically. Both relations above were confirmed by our numerical results. Then Eq. (30) may be rewritten as

$$\lambda_0\,(N_b, \tilde{\rho})\,/\sqrt{\zeta/a} = \sqrt{\tilde{\rho}}\,(b_2 - c_2\ \tilde{\rho})\,, \qquad (32)$$

which describes very well the behavior observed in Fig. 12 before the Mott insulator appears in the middle of the system. This is shown in Fig. 12 by a fit to our numerical results for $N = 1000$ with $b_2 = 1.44$ and $c_2 = 0.26$.

V. HARD-CORE BOSONS TRAPPED IN OTHER CONFINING POTENTIALS

The results obtained in the previous section for HCB's confined in harmonic traps can be generalized for arbitrary powers of the confining potential when the appropriate length scale,

$$\zeta = (V_\alpha/t)^{-1/\alpha}\,, \qquad (33)$$

is considered. [α is the power of the confining potential in Eq. (1)]. In this section, we perform systematically the generalization for a power $\alpha = 8$ of the confining potential in order to show that the statement above holds.

It has been already shown in Ref. [33] that density profiles as a function of the scaled positions in the trap (x/ζ) do not change when parameters in the system are changed keeping the characteristic density constant. This holds for any power of the confining potential. We start this section showing that the scaling of the lowest natural orbital, defined by [Eq. (23)] for the harmonic case ($\alpha = 2$), also holds for $\alpha = 8$. In Fig. 17, we compare the scaled two lowest natural orbitals for systems with different filling but the same characteristic density. φ was defined like in Eq. (23) with $\zeta = (V_8/t)^{-1/8}$, as corresponds to $\alpha = 8$. (Density profiles were included as thin dotted lines.) The plots show that indeed the scaling defined holds.

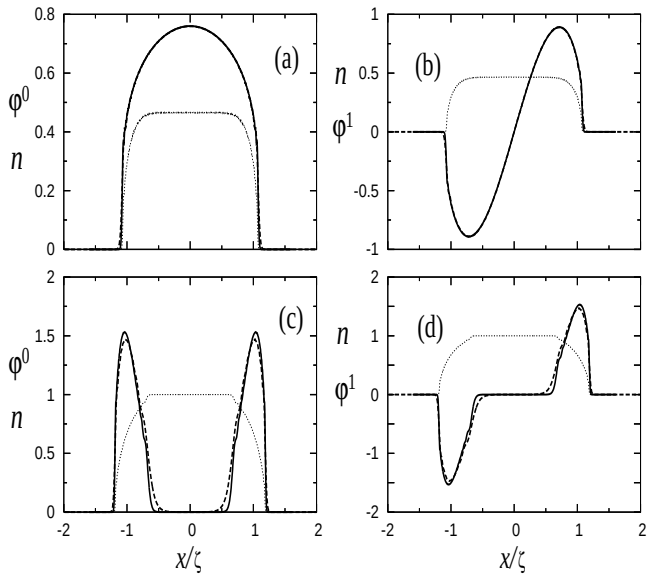


FIG. 17: Profiles of the two lowest natural orbitals for trapped systems with 700 lattice sites, $V_8 a^8 = 2.0 \times 10^{-19} t$, and occupations of 201 (a),(b) and 451 (c),(d) HCB's (continuous line); 300 lattice sites, $V_8 a^8 = 1.0 \times 10^{-15} t$, and occupations of 69 (a),(b) and 155 (c),(d) HCB's (dashed line). The density profiles have been included as thin dotted lines.

A. Off-diagonal correlations and the lowest natural orbital occupation

The increase of the power α of the confining potential leads to the formation of more homogeneous density profiles, as shown in Fig. 17. The fast changes of the density are restricted to smaller regions in the borders of the system. In Fig. 18, it can be seen that also for these systems off-diagonal quasi-long-range correlations are present in the one-particle density matrix. Like for the harmonic case, they decay as power laws $\rho_{ij} \sim |(x_i - x_j)/a|^{-1/2}$ for large distances and away from $n_i, n_j = 0, 1$. In the figure, we show results for a very dilute case, and for a trap with a density $n_i \sim 0.5$ in the middle of the system. A detailed study shows that like in the harmonic case, ρ_{ij} and $|(x_i - x_j)/a|^{-1/2}$ are related by a slowly varying (away from $n_i, n_j = 0, 1$) function of the density. We find this function, which we denote as $f_8(n_i, n_j)$, to depart at high densities from the $f_2(n_i, n_j)$ [Eq. (26)] behavior found in the harmonic case, i.e., the functional dependence of ρ_{ij} on the density *is not* universal. This can be seen in Fig. 19 where we plot ρ'_{ij} [Eq. (25)] vs n_j for two different values of n_i, and compare the results with $0.58[n_j(1 - n_j)]^{1/4}$. The differences between the plots start to be evident for large densities.

Considering the results above for the power-law decay of the one-particle density matrix and for the scaling of the lowest natural orbitals, it is possible to generalize for arbitrary powers of the confining potential the result obtained in the previous section for the occupation of the lowest natural orbital in the harmonic case [Eq.

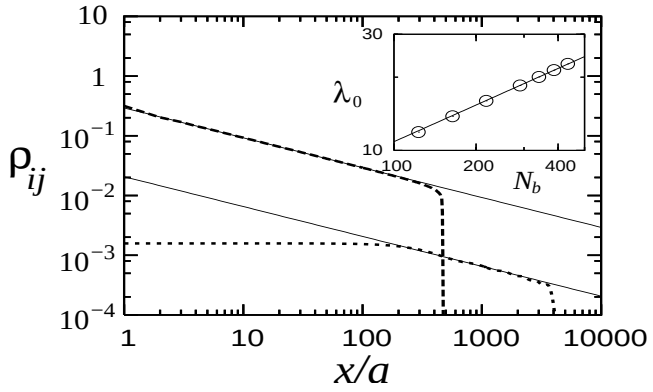


FIG. 18: HCB one-particle density matrix vs x/a ($x =\mid x_i - x_j \mid$) for systems with $N_b = 400$, $\tilde{\rho} = 0.92$, $n_i = 0.46$ (dashed line), and for a very dilute system with $N_b = 11$, $\tilde{\rho} = 7.56 \times 10^{-4}$, $n_i = 1.6 \times 10^{-3}$ (dotted line). The point i was chosen in the middle of the trap and only j was changed. The abrupt reduction of ρ_{ij} occurs for $n_j \to 0$. Thin continuous lines correspond to power laws $\sqrt{x/a}$. The inset shows λ_0 vs N_b for systems with $\tilde{\rho} = 1$ (◯), the straight line exhibits $\sqrt{N_b}$ behavior.

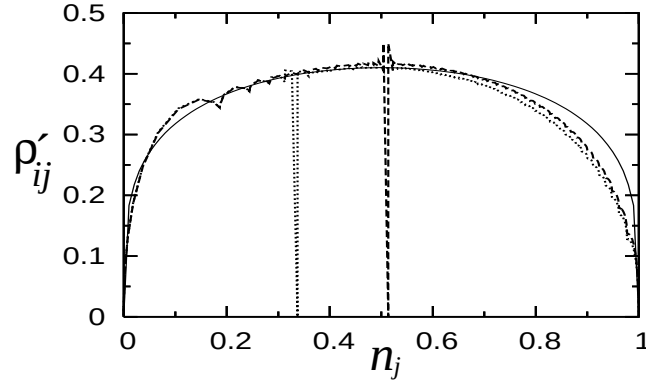


FIG. 19: HCB one-particle density matrix ρ'_{ij} [Eq. (25)] vs n_j. ρ'_{ij} is measured from points i with $n_i = 0.51$ (dashed line) and $n_j = 0.34$ (dotted line) in a trap with $\alpha = 8$, $N_b = 999$, and $\tilde{\rho} = 2.05$ so that a Mott insulator is formed in the middle of the system. The thin continuous line corresponds to $0.58[n_j(1-n_j)]^{1/4}$, like in Fig. 10.

(28)]. The differences between $f_8(n_i, n_j)$, $f_2(n_i, n_j)$, and eventually an arbitrary $f_\alpha(n_i, n_j)$ do not change the final result in Eq. (28) since density profiles as a function of the scaled positions x/ζ are unchanged when the characteristic density is kept constant. Then, independently of the power α of the trapping potential in Eq. (1), the occupation of the lowest natural orbital is determined in the thermodynamic limit as

$$\lambda_0^\alpha = C_\alpha(\tilde{\rho})\sqrt{N_b} = D_\alpha(\tilde{\rho})\sqrt{\zeta/a}\ , \qquad (34)$$

where $C_\alpha(\tilde{\rho})$ and $D_\alpha(\tilde{\rho})$ are functions of $\tilde{\rho}$ for a given power of the confining potential α. The thermodynamic limit is defined keeping the characteristic density $\tilde{\rho} = N_b/\zeta$ constant with ζ given by Eq. (33). As for the periodic and harmonic cases, the scaling in the thermodynamic limit is valid up to a good approximation for finite-size systems, as is shown in the inset in Fig. 18 for $\alpha = 8$ and $N_b > 100$.

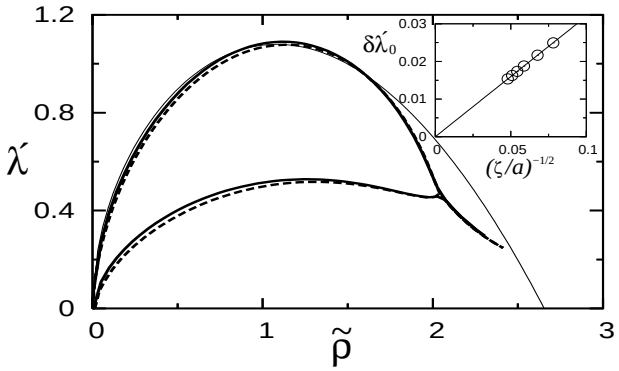


FIG. 20: Normalized occupation of the two lowest natural orbitals (see text) vs $\tilde{\rho}$. The systems analyzed have $N = 700$, $V_8 a^8 = 2 \times 10^{-19} t$, and occupations up to 501 particles (thick continuous line), and $N = 300$, $V_8 a^8 = 1.0 \times 10^{-15} t$, and occupations up to 181 particles (dashed line). The thin continuous line shows a fit of Eq. (37), with $b_8 = 1.36$ and $c_8 = 0.29$, to our numerical results for $N = 700$ ($\gamma = 8/5$ for $\alpha = 8$). The inset displays $\delta\lambda'_0$ vs $(\zeta/a)^{-1/2}$ (see text) for $\tilde{\rho} = 1.0$ (◯), the continuous line shows the result of our fits.

A global picture of the occupation of the two lowest natural orbitals in the case $\alpha = 8$ is shown in Fig. 20(a). There we plot $\lambda' = \lambda/\sqrt{\zeta/a}$ vs $\tilde{\rho}$, like in the harmonic case (Fig. 12), and compare systems with different curvatures of the confining potential. The Mott insulator appears in the middle of the trap when the degeneracy of the natural orbitals sets in. The comparison between the plots shows that also for $\alpha = 8$ and the system sizes chosen, finite-size corrections are small. In the following we check whether they have the same functional form as for the homogeneous and harmonically trapped cases. The inset in Fig. 20 shows that this is indeed the case. We assume that $\lambda_0/\sqrt{\zeta/a} = C_8(\tilde{\rho}) - D_8(\tilde{\rho})/\sqrt{\zeta/a}$, like for the harmonic trap [Eq. (29)], and calculate $C_8(\tilde{\rho})$ and $D_8(\tilde{\rho})$. In the inset in Fig. 20, we plot $\delta\lambda'_0 = C_8(\tilde{\rho}) - \lambda_0/\sqrt{\zeta/a}$ vs $(\zeta/a)^{-1/2}$ for $\tilde{\rho} = 1$, the linear behavior observed confirms our assumption.

B. Low-density limit in the lattice

In the following, we analyze the corrections introduced by the lattice to the occupation of the lowest natural orbitals in the confined continuous case. For a trap with power $\alpha = 8$ of the confining potential, it can be proven numerically (Fig. 21) that in the low-energy region the ratio between the level spacing and the bandwidth reduces proportionally to $(V_8 a^8/t)^{1/5}$, i.e., proportionally to $(\zeta/a)^{-8/5}$. As for the periodic and harmonically trapped systems, we find that the lowest natural orbital occupations approach their value in the continuous system $\Lambda_\eta(N_b)$ following the same behavior,

$$\lambda_\eta(N_b, \zeta/a) = \Lambda_\eta(N_b) - E_\eta^8(N_b)(\zeta/a)^{-8/5}. \qquad (35)$$

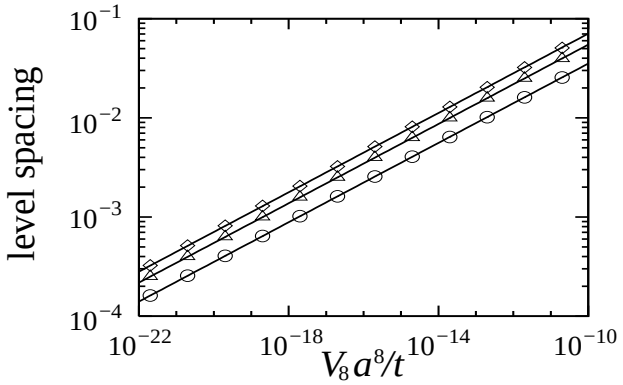


FIG. 21: Level spacing (in units of t) vs $V_8 a^8/t$. (◯) between first and second level, (△) between second and third level, and (◇) between third and fourth level. The lines following the data correspond to power laws $(V_8 a^8/t)^{0.2}$.

We calculate $\Lambda_\eta\,(N_b)$ and $E^8_\eta\,(N_b)$ for the three lowest natural orbitals analyzing systems with fillings up to 401 particles and sizes up to 2000 lattice sites. The results obtained are shown in Figs. 22(a) and 22(b), respectively. In Fig. 22 we compare our results for $\Lambda_\eta\,(N_b)$ and $E^8_\eta\,(N_b)$ with the power laws expected from comparing Eq. (35) and Eq. (34), i.e.,

$$\Lambda_\eta\,(N_b) = b_8\ \sqrt{N_b}, \qquad E_8\,(N_b) = c_8\ N_b^{21/10} \tag{36}$$

The plots show that for large occupations, basically larger that 100 HCB's, the expected power laws are observed. In addition, we plot as an inset in Fig. 22(b) $\Delta\lambda = \Lambda_\eta\,(N_b) - \lambda_\eta\,(N_b, \zeta/a)$ also for the three lowest natural orbitals as a function of $(\zeta/a)^{-8/5}$. These plots show that the scaling behavior proposed in Eq. (35) is correct. We also find that like in the harmonic trap, Eq. (35) follows the numerical results up to fillings very close to the one at which the Mott insulator appears in the middle of the system. Equation (35) can be rewritten for the lowest natural orbital as

$$\lambda_0\,(N_b, \zeta/a) = \sqrt{N_b}\,(b_8 - c_8\ \tilde{\rho}^{\gamma}) \tag{37}$$

with $\gamma = 8/5$. Similar expressions were obtained for the periodic (changing $\tilde{\rho}$ by ρ) [Eq. (21)] and harmonically trapped [Eq. (32)] systems, with $\gamma = 2$ and $\gamma = 1$, respectively. As is shown in Fig. 20, Eq. (37) (with $\gamma = 8/5$) describes very well our numerical results below $\tilde{\rho} = 2$ for the following fitting parameters: $b_8 = 1.36$ and $c_8 = 0.29$.

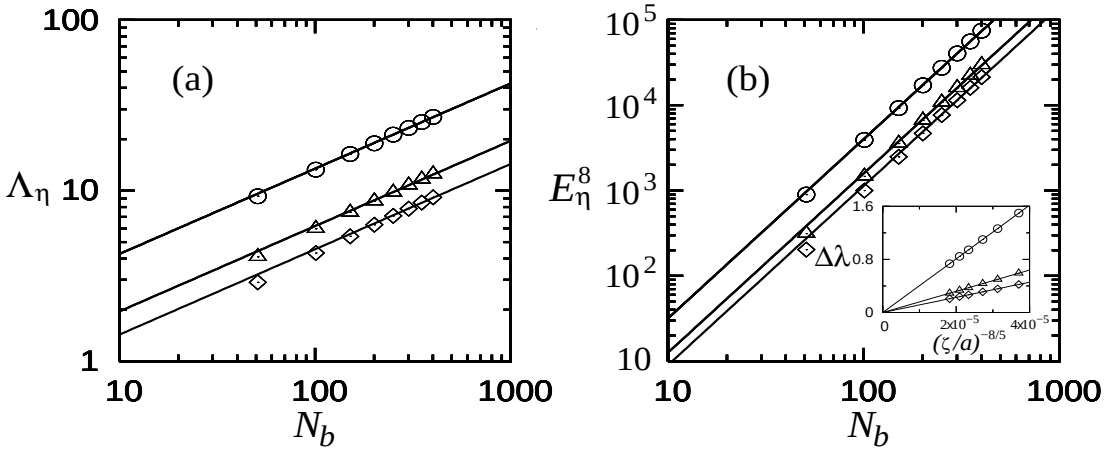


FIG. 22: Values obtained for $\Lambda_\eta\,(N_b)$ (a) and $E^8_\eta\,(N_b)$ (b) vs N_b, for the first (◯), second (△), and third (◇) natural orbitals. The lines following the data correspond to power laws $\sqrt{N_b}$ (a) and $N_b^{21/10}$ (b). The inset in (b) shows $\Delta\lambda$ (see text) as a function of $(\zeta/a)^{-8/5}$ also for the first (◯), second (△), and third (◇) natural orbitals in systems with 301 HCB's and sizes between 1000 and 2000 lattice sites.

VI. CONCLUSIONS

We have studied in detail ground-state properties of hard-core bosons confined on 1D lattices. The results obtained for the off-diagonal behavior of the one-particle density matrix show that it decays with the same power law known from periodic systems [25], independently of the power of the confining potential. In contrast, we find that the small dependence of the one-particle density matrix on the density is not universal. In the harmonically trapped case we were able to find a function that fits very well this density dependence [Eq. (24)]. The results we have obtained for HCB's are equally valid for the 1D XY model with a space-varying transverse field.

We have shown how the occupation of the lowest natural orbital is set by the large distance behavior of the one-particle density matrix. Even in the cases where a

region with $n_i = 1$ builds up in the middle of the system, we find that this quantity scales proportionally to the square root of the number of particles (at constant characteristic density), and independently of the power of the confining potential. The functional form of the constant of proportionality, as a function of the characteristic density, was determined for fillings below the one at which the Mott insulating region appears in the density profiles. We have also obtained the first correction to the square-root behavior of the lowest natural orbital occupation due to finite-size effects. We find that it is also universal independent of the power of the confining potential. Although not discussed here, we should mention that the natural orbital occupations λ_η also display another universal behavior for large values of η at low densities $\lambda_\eta \sim \eta^{-4}$, a behavior that is shared by the momentum distribution function for large momenta $n_k \sim |k|^{-4}$ [29].

Finally, we studied systematically the low-density limit in a lattice. We have shown how the results for the occupation of the lowest natural orbitals in continuous systems can be obtained as an extrapolation in a lattice. The only input knowledge ones needs to do this extrapolation is the behavior of the ratio between the level spacing and the bandwidth for the lowest energy levels as a function of the strength of the confining potential.

Acknowledgments

We would like to thank HLR-Stuttgart (Project DynMet) for allocation of computer time and SFB 382 for financial support. We are grateful to S. Wessel for useful discussions.

[1] J. H. Thywissen, R. M. Westervelt, and M. Prentiss, Phys. Rev. Lett. **83**, 3762 (1999).
[2] D. Müller, D. Z. Anderson, R. J. Grow, P. D. D. Schwindt, and E. A. Cornell, Phys. Rev. Lett. **83**, 5194 (1999).
[3] N. H. Dekker, C. S. Lee, V. Lorent, J. H. Thywissen, S. P. Smith, M. Drndic, R. M. Westervelt, and M. Prentiss, Phys. Rev. Lett. **84**, 1124 (2000).
[4] M. Key, I. G. Hughes, W. Rooijakkers, B. E. Sauer, E. A. Hinds, D. J. Richardson, and P. G. Kazansky, Phys. Rev. Lett. **84**, 1371 (2000).
[5] K. Bongs, S. Burger, S. Dettmer, D. Hellweg, J. Arlt, W. Ertmer, and K. Sengstock, Phys. Rev. A **63**, 031602(R) (2001).
[6] F. Schreck, L. Khaykovich, K. L. Corwin, G. Ferrari, T. Bourdel, J. Cubizolles, and C. Salomon, Phys. Rev. Lett. **87**, 080403 (2001).
[7] A. Görlitz, J. M. Vogels, A. E. Leanhardt, C. Raman, T. L. Gustavson, J. R. Abo-Shaeer, A. P. Chikkatur, S. Gupta, S. Inouye, T. Rosenband, and W. Ketterle, Phys. Rev. Lett. **87**, 130402 (2001).
[8] M. Greiner, I. Bloch, O. Mandel, T. W. Hänsch, and T. Esslinger, Phys. Rev. Lett. **87**, 160405 (2001).
[9] H. Moritz, T. Stöferle, M. Köhl, and T. Esslinger, Phys. Rev. Lett. **91**, 250402 (2003).
[10] T. Stöferle, H. Moritz, C. Schori, M. Köhl, and T. Esslinger, Phys. Rev. Lett. **92**, 130403 (2004).
[11] M. Olshanii, Phys. Rev. Lett. **81**, 938 (1998).
[12] D. S. Petrov, G. V. Shlyapnikov, and J. T. M. Walraven, Phys. Rev. Lett. **85**, 3745 (2000).
[13] V. Dunjko, V. Lorent, and M. Olshanii, Phys. Rev. Lett. **86**, 5413 (2001).
[14] M. Girardeau, J. Math. Phys. **1**, 516 (1960).
[15] A. Lenard, J. Math. Phys. **5**, 930 (1964); *ibid.* **7**, 1268 (1966).
[16] H. G. Vaidya and C. A. Tracy, Phys. Rev. Lett. **42**, 3 (1979).
[17] M. D. Girardeau, E. M. Wright, and J. M. Triscari, Phys. Rev. A **63**, 033601 (2001).
[18] A. Minguzzi, P. Vignolo, and M. P. Tosi, Phys. Lett. A **294**, 222 (2002).
[19] G. J. Lapeyre, M. D. Girardeau, and E. M. Wright, Phys. Rev. A **66**, 023606 (2002).
[20] T. Papenbrock, Phys. Rev. A **67**, 041601(R) (2003).
[21] P. J. Forrester, N. E. Frankel, T. M. Garoni, and N. S. Witte, Phys. Rev. A **67**, 043607 (2003).
[22] D. M. Gangardt, J. Phys. A **37**, 9335 (2004).
[23] B. Paredes, A. Widera, V. Murg, O. Mandel, S. Fölling, I. Cirac, G. V. Shlyapnikov, T. W. Hänsch, and I. Bloch, Nature (London) **429**, 277 (2004).
[24] E. Lieb, T. Shultz, and D. Mattis, Ann. Phys. (N.Y.) **16**, 407 (1961).
[25] B. M. McCoy, Phys. Rev. **173**, 531 (1968).
[26] H. G. Vaidya and C. A. Tracy, Phys. Lett. **68**A, 378 (1978).
[27] B. M. McCoy, J. H. Perk, and R. E. Schrock, Nucl. Phys. B **220**, 35 (1983); *ibid.* **220**, 269 (1983).
[28] P. Jordan and E. Wigner, Z. Phys. **47**, 631 (1928).
[29] M. Rigol and A. Muramatsu, Phys. Rev. A **70**, 031603(R) (2004).
[30] M. Rigol and A. Muramatsu, Phys. Rev. Lett. **93**, 230404 (2004).
[31] M. Rigol and A. Muramatsu, Phys. Rev. A **70**, 043627 (2004).
[32] M. Rigol, A. Muramatsu, G. G. Batrouni, and R. T. Scalettar, Phys. Rev. Lett. **91**, 130403 (2003).
[33] M. Rigol and A. Muramatsu, Phys. Rev. A **69**, 053612 (2004).
[34] O. Penrose and L. Onsager, Phys. Rev. **104**, 576 (1956).
[35] C. Kollath, U. Schollwöck, J. von Delft, and W. Zwerger, Phys. Rev. A **69**, 031601(R) (2004).
[36] S. Wessel, F. Alet, M. Troyer, and G. G. Batrouni, Phys. Rev. A **70**, 053615 (2004).
[37] G. G. Batrouni, V. Rousseau, R. T. Scalettar, M. Rigol, A. Muramatsu, P. J. H. Denteneer, and M. Troyer, Phys. Rev. Lett. **89**, 117203 (2002).